Journal of Alloys and Compounds 509 (2011) 9144–9149

Contents lists available at ScienceDirect

Journal of Alloys and Compounds

journal homepage: www.elsevier.com/locate/jallcom

Controllable synthesis of bifunctional $NaYF_4:Yb^{3+}/Ho^{3+}@SiO_2/Au$ nanoparticles with upconversion luminescence and high X-ray attenuation

Zhijiang Wang[a,*], Lina Wu[b], Huijuan Liang[c], Wei Cai[d], Zhiguo Zhang[c], Zhaohua Jiang[a]

[a] School of Chemical Engineering and Technology, Harbin Institute of Technology, Harbin 150001, China
[b] Department of Medical Imaging and Nuclear Medicine, Molecular Imaging Center, The Fourth Affiliated Hospital, Harbin Medical University, Harbin 150001, China
[c] Department of Physics, Harbin Institute of Technology, Harbin 150001, China
[d] School of Materials Science and Engineering, Harbin Institute of Technology, Harbin 150001, China

ARTICLE INFO

Article history:
Received 21 May 2011
Received in revised form 19 June 2011
Accepted 21 June 2011
Available online 14 July 2011

Keywords:
Bifunctional nanoparticles
Upconversion nanocrystal
Gold nanoparticles
Upconversion luminescence
X-ray attenuation

ABSTRACT

A novel type of bifunctional water-soluble $NaYF_4:Yb^{3+}/Ho^{3+}@SiO_2/Au$ nanocomposite is fabricated by a facile layer-by-layer technology in which the mercapto–silica shell is used as the functional layer coating on the central $NaYF_4:Yb^{3+}/Ho^{3+}$ nanocrystals. Then by adjusting the mole ratio of the Au nanoparticles to the $NaYF_4:Yb^{3+}/Ho^{3+}@SiO_2$ nanoparticles, control of the gold loading on the upconversion nanocrystal surface is achieved. The fabricated nanocomposites inherit the excellent physical and chemical properties from their building blocks, simultaneously exhibiting upconversion luminescence and high X-ray attenuation and as well are easily modified with various molecules. These properties render the synthesized $NaYF_4:Yb^{3+}/Ho^{3+}@SiO_2/Au$ nanocomposite not only useful as a multimodality contrast agent to increase the efficiency of molecular imaging but also has the potential of in situ curing of diseases.

1. Introduction

Multicomponent nanostructures that contain two or more different nanoscale functionalities are attractive candidates for advanced nanomaterials [1–5]. With controlled structure and interface interactions, these nanocomposites can inherit excellent chemical and physical properties from their parent components, which greatly enhance the potential and broaden the application of such composite bifunctional nanomaterials in the areas of biotechnology, electronics, photonics, catalysis, and sensors.

Nanoparticles derived from lanthanide-doped upconversion (UC) nanocrystals, which can convert a long wavelength radiation (e.g., NIR light) to a short wavelength fluorescence (e.g., visible light) via a two-photon or multiphoton mechanism, have attracted a great deal of attention because of their superior spectroscopic properties [6–8]. Compared to the organic fluorophores and quantum dots, lanthanide-doped UC nanocrystals exhibit long fluorescence lifetimes, low photobleaching, high quantum yields, narrow emission peak, and large Stokes shifts. Furthermore, their low autofluorescence background, high chemical stability, and tunable optical property by varying lanthanide dopants make such nanoparticles suitable for fluorescence labeling [9–14]. However, most UC nanocrystals are prepared using high-temperature routes. They have no intrinsic aqueous solubility and a lack of functional moieties, which greatly limits their applications in biotechnology. The silica coating can endow UC nanocrystals with superior colloidal properties and facilitate the subsequent functionalization, which makes UC nanocrystals strong candidates for application in biological labeling.

On the other hand, metal nanoparticles, especially gold nanoparticles, have been extensively studied in the fields of biomedical applications, including biosensors [15,16], biomedical diagnostics [17], and drug delivery [18]. This is not only because gold nanoparticles are compatible with biological molecules and high chemical stability [19,20], but also due to their exceptional optical properties, high X-ray attenuation and various modification means [21–23]. If one specific kind of nanocomposites could possess both the UC luminescence and high X-ray attenuation as well as easily link up with various agents and molecules on the surface, it would greatly broaden the applications of nanomaterials in biomedical fields. Herein, we present the report on fabricating such nanocomposites, $NaYF_4:Yb^{3+}/Ho^{3+}@SiO_2/Au$, where via a facile layer-by-layer technology in which a mercapto–silica shell is utilized as a functional layer on the central UC nanocrystals and then by the adjustment of the mole ratio of the building blocks, control of gold loading can be achieved. The fabricated nanocomposites, inheriting excellent physicochemical properties from the building blocks, possess UC luminescence and high X-ray attenuation and at the same time easily link up with various agents and molecules on the surface.

* Corresponding author. Tel.: +86 451 86402805; fax: +86 451 86402805.
E-mail address: wangzhijiang@hit.edu.cn (Z. Wang).

0925-8388/$ – see front matter © 2011 Elsevier B.V. All rights reserved.
doi:10.1016/j.jallcom.2011.06.088

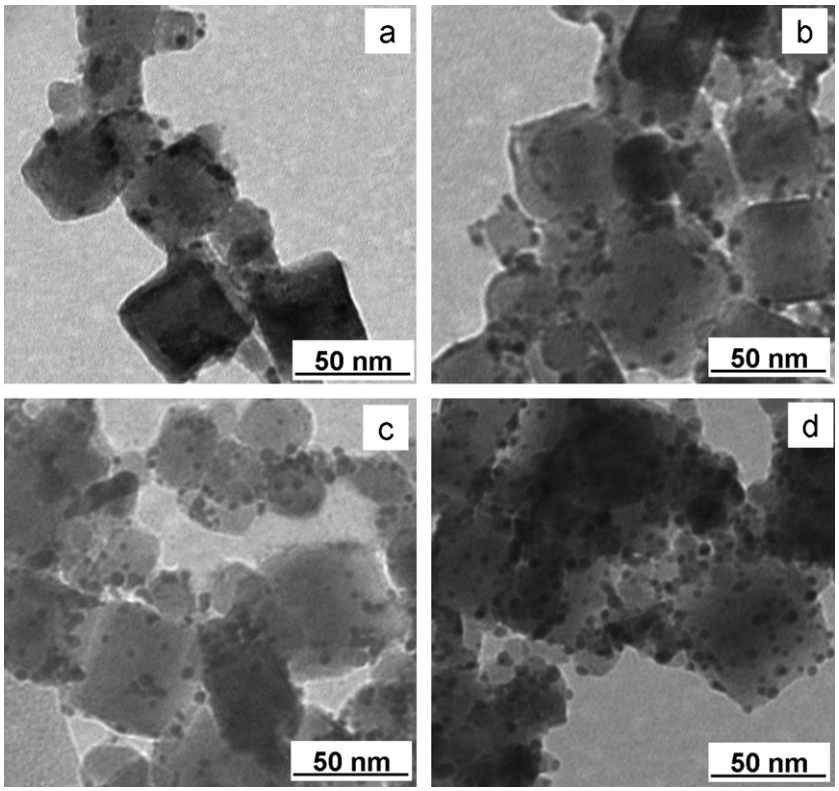

Fig. 1. TEM images of nanocomposites (a) sample CN1, (b) sample CN2, (c) sample CN3, and (c) sample CN4.

2. Material and methods

2.1. Materials

Hydrogen tetrachloroaurate trihydrate ($HAuCl_4{\cdot}3H_2O$, 99.99%, ACS reagent grade) from Alfa, sodium borohydride ($NaBH_4$, 99%), tetraethoxy silane (TEOS, 99%), 3-mercaptopropyltrimethoxysilane (MPTMS, 95%), yttrium oxide (Y_2O_3, 99.99%), ytterbium oxide (Yb_2O_3, 99.99%) and holmium oxide (Ho_2O_3, 99.99%) from Aldrich were used as received. Deionized water with high resistivity (18.2 MΩ cm) was obtained through a TKA GenPure ultrapure water system. All the glassware was thoroughly cleaned with aqua regia (HCl:HNO_3 = 3:1 vol%), rinsed with ultrapure water, and then dried in an oven prior to use.

2.2. Characterization

Transmission electron microscopy (TEM) images of samples were obtained on a Philips Tecnai G^2 electron microscope operated at 200 keV. X-ray diffraction (XRD) experiments were carried out on a Rigaku D/max-γB diffractometer equipped with a rotating anode and a Cu Kα source operated at 40 kV and 100 mA. UV–visible (UV–vis) absorption spectra were carried out by using a calibrated spectrophotometer (Cary 4000, Varian) at room temperature. The room temperature UC luminescence spectra were collected by a lens-coupled monochromator (Zolix Instruments Co. Ltd., Beijing) of 3-nm spectral resolution with an attached photomultiplier tube (Hamamatsu CR131) under excitation at 970 nm diode laser. Computed tomography (CT) measurement was carried out by employing a Toshiba Aquilion 64 CT Scanner with 400 mA and 120 kVp. Scanning was performed in the transverse axial plane using 0.5 mm slice-thickness. A uniform region of interest was carefully placed over the center of each vial containing the gold nanoparticles and nanocomposites dispersion to measure attenuation values.

2.3. Preparation of $NaYF_4$:Yb^{3+}/Ho^{3+} nanocrystals

Nanocrystals $NaYF_4$ doped with 2 mol% Ho^{3+} and 20 mol% Yb^{3+} ions were synthesized by a hydrothermal process. In a typical synthesis, NaOH (1.0 g, 25 mmol), water (5 mL), ethanol (5 mL), and oleic acid (15 mL) were mixed under agitation to form a homogeneous solution. Then 1.2 mmol (total amounts) of rare-earth chloride ($Ho(NO_3)_3$, $Yb(NO_3)_3$ and $Y(NO_3)_3$) aqueous solution were added under magnetic stirring with the (Ho^{3+} + Yb^{3+} + Y^{3+})/NaF molar ratio being 1:4. Subsequently, aqueous NaF solution was added dropwise to the above solution. The mixture was agitated for about 10 min, then transferred to a 50 mL autoclave, sealed, and hydrothermally treated at 180 °C for 18 h. The system was cooled to room-temperature naturally, and the products were deposited at the bottom of the vessel. Cyclohexane was employed to dissolve and collect the products. Pure powders were obtained by purifying the samples with ethanol several times to remove oleic acid, sodium oleic, and other remnants.

2.4. Coating NaYF4:Yb^{3+}/Ho^{3+} nanocrystals with mercapto–silica shell

Typically, 125 mg of $NaYF_4$:Yb^{3+}/Ho^{3+} nanocrystals were dispersed in 100 mL of cyclohexane by sonication. After the addition of 1.25 mL of 25% ammonia and 50 μL of TEOS, the mixture was stirred for 6 h. Then 70 μL of MPTMS was added into the mixture. After further stirring for 6 h, the solvent was removed by decantation after centrifugation (12,000 rpm) for 5 min. The precipitate was washed three times with acetone through an ultrasonic redispersion–centrifugation process to remove the impurities. Lastly, the precipitate was suspended in an aqueous solution.

2.5. Synthesis of gold nanoparticles

Gold nanoparticles were prepared following the previous report with some modification [24]. Firstly, a 20 mL aqueous solution containing 0.25 mM $HAuCl_4$ and 0.25 mM trisodium citrate was prepared. Next, 0.6 mL of 0.05 M $NaBH_4$ solution was added all at once into the gold salt solution under constant stirring. Stirring was continued for another 60 s. The resulting solution turned a wine red color indicating the formation of gold nanoparticles.

2.6. Fabrication of $NaYF_4$:Yb^{3+}/Ho^{3+}@SiO_2/Au nanocomposites

Firstly, the as-prepared $NaYF_4$:Yb^{3+}/Ho^{3+}@SiO_2 colloidal solution was put into an ultrasonic apparatus. Then, the gold colloidal solution was dropped into the above solution under ultrasonication. After 15 min, the $NaYF_4$:Yb^{3+}/Ho^{3+}@SiO_2/Au nanocomposites were collected with an ultrasonic redispersion–centrifugation process. Under 12,000 rpm centrifugation, the nanocomposites were precipitated, while free gold nanoparticles remained in the solvent. This procedure was repeated twice. The obtained $NaYF_4$:Yb^{3+}/Ho^{3+}@SiO_2/Au nanocomposites were then dispersed in aqueous solution for later use.

3. Results and discussion

Controlled attachment of Au nanoparticles onto mercapto–silica coated UC nanocrystals. The strategy for the fabrication of bifunctional $NaYF_4$:Yb^{3+}/Ho^{3+}@SiO_2/Au nanocomposites is illustrated in Scheme 1. Firstly, the UC nanocrystals, $NaYF_4$:Yb^{3+}/Ho^{3+}, were

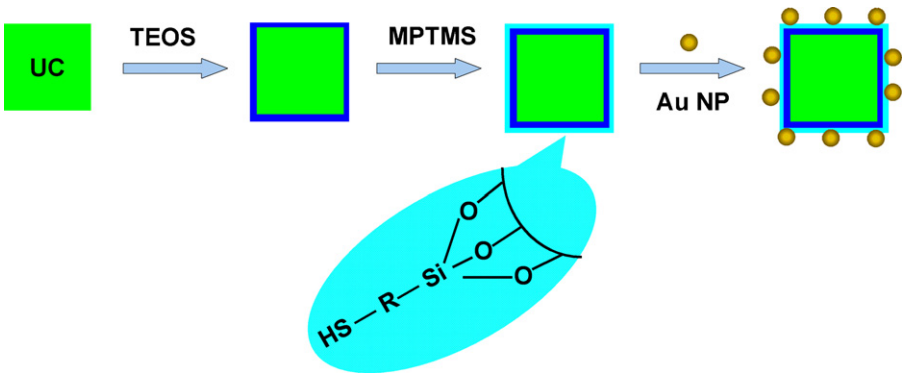

Scheme 1. Schematic illustration for the fabrication procedure of $NaYF_4:Yb^{3+}/Ho^{3+}@SiO_2$/Au nanocomposites. UC = upconversion nanocrystals, TEOS = tetraethoxy silane, MPTMS = 3-mercaptopropyltrimethoxysilane, NP = nanoparticles.

prepared by a hydrothermal route. In the course of the reaction, oleic acid molecules were coated onto the outer face of the in situ generated UC nanocrystals through the interaction between rare-earth ions and carboxyl groups of oleic acids, with the hydrophobic alkyl chains left outside. All the UC nanocrystals produced were easily dispersed in a nonpolar solvent. To convert the hydrophobic nanocrystals into hydrophilic analogues and to have the ability of tightly linking with gold nanoparticles, a sol-gel process based on a modified Stöber method was utilized to form a mercapto–silica shell on the surface of $NaYF_4:Yb^{3+}/Ho^{3+}$ nanocrystals. Lastly, the thiol-modified $NaYF_4:Yb^{3+}/Ho^{3+}@SiO_2$ colloids were mixed with citrate-stabilized Au nanoparticles under ultrasonic conditions. Bifunctional nanocomposites were obtained by this process. The code and materials molar ratio in the synthesis of $NaYF_4:Yb^{3+}/Ho^{3+}@SiO_2$/Au nanocomposites are presented in Table 1. Qualitative evidence of controlled gold loading is observed in a series of TEM images in Fig. 1, showing the increase of particle surface coverage with gold nanoparticles as a result of increased relative concentration ratio of gold nanoparticles to $NaYF_4$ nanocrystals.

The composition and crystallinity of the as-synthesized $NaYF_4:Yb^{3+}/Ho^{3+}@SiO_2$/Au nanocomposites was checked with X-ray diffraction technology and compared with $NaYF_4:Yb^{3+}/Ho^{3+}$ nanocrystals. There are nine major diffraction peaks at 28.28°, 32.80°, 46.88°, 55.72°, 58.62°, 68.74°, 75.58°, 77.98°, and 87.24° observed for the $NaYF_4:Yb^{3+}/Ho^{3+}$ nanocrystals (Fig. 2a), which can be assigned to (111), (200), (220), (311), (222), (400), (331), (420), and (422) planes of the face-centered cubic (fcc) $NaYF_4$ (JCPDS card no. 77-2042), respectively. In the case of $NaYF_4:Yb^{3+}/Ho^{3+}@SiO_2$/Au nanocomposites, the peaks of fcc $NaYF_4$ are observed in the nanocomposites (Fig. 2b), revealing that the surface-modified UC nanocrystals do not change their phases, and four additional diffraction peaks at 38.20°, 44.42°, 64.58°, and 78.02° representing Bragg reflection from (111), (200), (220), and (311) planes of Au are also observed (JCPDS card no. 04-0784). This indicates that the gold nanoparticles do exist in the $NaYF_4:Yb^{3+}/Ho^{3+}@SiO_2$/Au nanocomposites.

The TEM images and XRD results demonstrate that the fabrication procedure illustrated in Scheme 1 is a successful approach

Table 1
The code and materials mole ratio in synthesis of $NaYF_4:Yb^{3+}/Ho^{3+}@SiO_2$/Au nanocomposites.

Code	$NaYF_4:Yb^{3+}/Ho^{3+}@SiO_2$ nanoparticles (5×10^{-8} mol/L)	Au nanoparticles (1.4×10^{-10} mol/L)
CN1	2 mL	4 mL
CN2	1 mL	4 mL
CN3	0.5 mL	4 mL
CN4	0.2 mL	4 mL

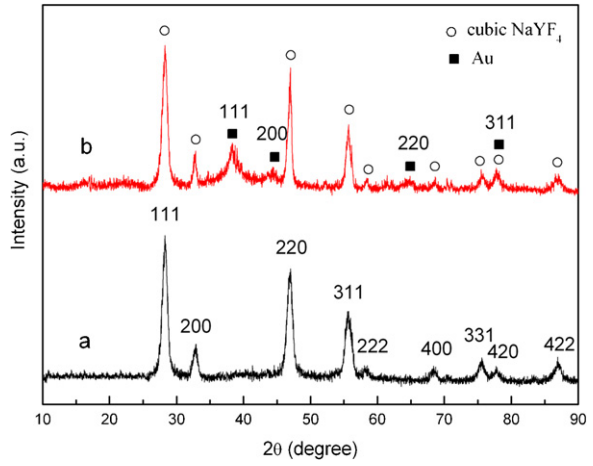

Fig. 2. XRD patterns of (a) $NaYF_4:Yb^{3+}/Ho^{3+}$ nanocrystals and (b) $NaYF_4:Yb^{3+}/Ho^{3+}@SiO_2$/Au nanocomposite CN4.

to synthesize multicomponent nanostructures in which the utilization of a mercapto–silica shell as a functional layer and the adjustment of the mole ratio of the building blocks allow control of gold loading.

The optical properties and X-ray attenuation of the $NaYF_4:Yb^{3+}/Ho^{3+}@SiO_2$/Au nanocomposites. Fig. 3 is the UV–vis

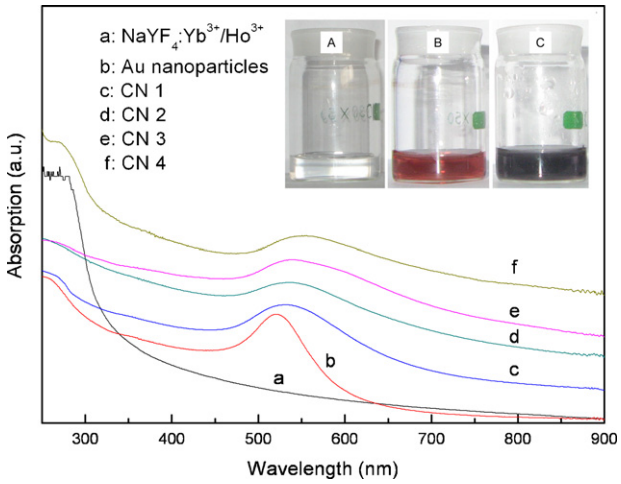

Fig. 3. UV–vis absorption spectra of $NaYF_4:Yb^{3+}/Ho^{3+}$ nanocrystals, gold nanoparticles, and $NaYF_4:Yb^{3+}/Ho^{3+}@SiO_2$/Au nanocomposites. The inset shows photograph of the aqueous solutions dispersed with (A) $NaYF_4:Yb^{3+}/Ho^{3+}@SiO_2$ nanoparticles, (B) gold nanoparticles and (C) $NaYF_4:Yb^{3+}/Ho^{3+}@SiO_2$/Au nanocomposite CN4.

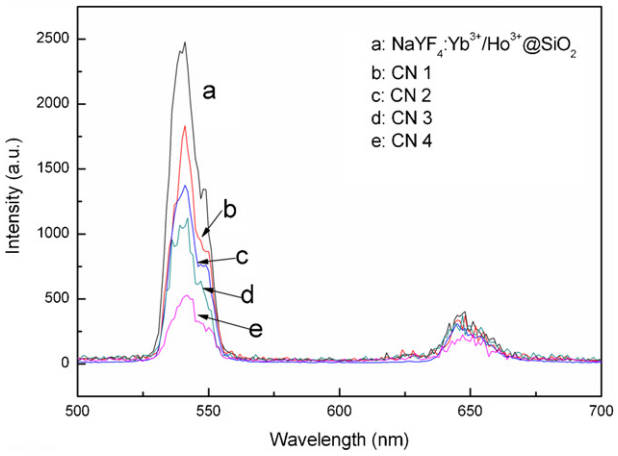

Fig. 4. Upconversion luminescence spectra of $NaYF_4$:Yb^{3+}/Ho^{3+}@SiO_2 nanoparticles and $NaYF_4$:Yb^{3+}/Ho^{3+}@SiO_2/Au nanocomposites.

spectra and colorimetric characteristics of the prepared 4.2-nm-sized Au nanoparticles, UC nanocrystals, and $NaYF_4$:Yb^{3+}/Ho^{3+}@SiO_2/Au nanocomposites. It is known that for gold nanoparticles in sizes ranging from 2 to 100 nm, the electrons are trapped in the small Au metal box and exhibit a characteristic of collective oscillation frequency of the plasmon resonance, giving rise to the plasmon resonance band at around 520 nm [25,26]. The exact absorption position varies with particle size and interparticles distance. The absorption peak at 521 nm for the prepared Au nanoparticles was observed. Once gold nanoparticles are attached to $NaYF_4$:Yb^{3+}/Ho^{3+}@SiO_2 nanoparticles, their absorption bands broaden and undergo a gradual red shift. The shifting in the UV–vis absorption spectra is due to the strong interparticle interaction and the coupling of the surface plasmon of neighbouring gold nanoparticles. From the inset photograph of Fig. 3, we can clearly see the color change of $NaYF_4$:Yb^{3+}/Ho^{3+}@SiO_2 colloidal solution before and after Au conjugation. The original color of $NaYF_4$:Yb^{3+}/Ho^{3+}@SiO_2 colloidal solution is transparent, and the Au colloidal solution is red-purple. The resulting $NaYF_4$:Yb^{3+}/Ho^{3+}@SiO_2/Au colloidal solution exhibits a blue-purple color, indicating that the nanocomposites have inherited the plasmon absorption of gold nanoparticles.

Fig. 4 presents the UC luminescence emissions of $NaYF_4$:Yb^{3+}/Ho^{3+}@SiO_2 nanoparticles and the four prepared nanocomposites samples. Under excitation at 970 nm, two UC emission peaks at 541 and 647 nm are observed for all the samples, which arise from the 4f configuration transitions of Ho^{3+} from $^5S_2/^5F_4$ and $^5F_5$ to the ground state $^5I_8$, respectively. In the nanocomposites, the interparticle communication between the nanoscale Au and $NaYF_4$:Yb^{3+}/Ho^{3+} leads to the change of UC luminescence intensity of the UC nanocrystals. With the increase of the gold content in the nanocomposites, a progressive quenching of the UC luminescence is observed. Although the UC luminescence intensity is decreased, the UC emission is still enough for the biolabeling when controlling gold in the proper content.

The quenching of UC luminescence can be induced by the change of UC luminescence mechanism [27], the increase of nonradiative decay rate and the decrease of the radiative rate [28]. Fig. 5 shows the pump power dependence of UC emission in the $NaYF_4$:Yb^{3+}/Ho^{3+}@SiO_2 nanoparticles and $NaYF_4$:Yb^{3+}/Ho^{3+}@SiO_2/Au nanocomposites CN1. The slope value represents the number of pump photons absorbed per shortwavelength photon emitted. As illustrated in Fig. 5a, the slope *n* value of 1.7 and 2.0 are observed for an emission in 541 and 647 nm, respectively, which suggests a two-proton process for the 541 and 647 nm emission in the $NaYF_4$:Yb^{3+}/Ho^{3+}@SiO_2 nanopaticles. Similarly, a two-proton UC mechanism is also involved to generate the UC emission in the $NaYF_4$:Yb^{3+}/Ho^{3+}@SiO_2/Au nanocomposites as presented in Fig. 5b. It is apparent that the attachment of gold nanoparticles does not change the UC luminescence mechanism of the UC nanocrystals.

It can be observed from Figs. 3 and 4 that the absorption of the nanocomposites matches closely with the UC emission of the nanocomposites at ~541 nm. According to the theory of fluorescence resonant energy transfer (FRET), when the absorption of the energy acceptor is close to the emission of the phosphor and when the donor and the acceptor are close enough, the emission of the energy donor will be quenched by the energy acceptor [29]. The distance between gold nanoparticles (energy acceptors) and UC nanocrystals (energy donors) is the thickness of the silica shell, being 2 nm. Thus, the FRET system is constructed in the $NaYF_4$:Yb^{3+}/Ho^{3+}@SiO_2/Au nanocomposites as shown in Fig. 6, which results in the UC luminescence quenching by the means of increasing nonradiative decay rate and decreasing radiative rate of the UC nanocrystals. When more gold nanoparticles are located on the nanocomposites, the energy transfer is enhanced and more quenching occurs.

The X-ray attenuation of the nanocomposites CN1 at different concentrations is examined on a CT scanner and compared with 4.2-nm-sized gold nanoparticles. Fig. 7 shows that the nanocomposites exhibit a higher X-ray attenuation than 4.2-nm-sized gold nanoparticles at the same gold concentration. This is the reason that compared to the single gold colloidal solution, the nanocomposites colloidal solution contains Y, Yb and Ho which also make X-ray attenuated [30]. It is known that gold nanoparticles have a higher

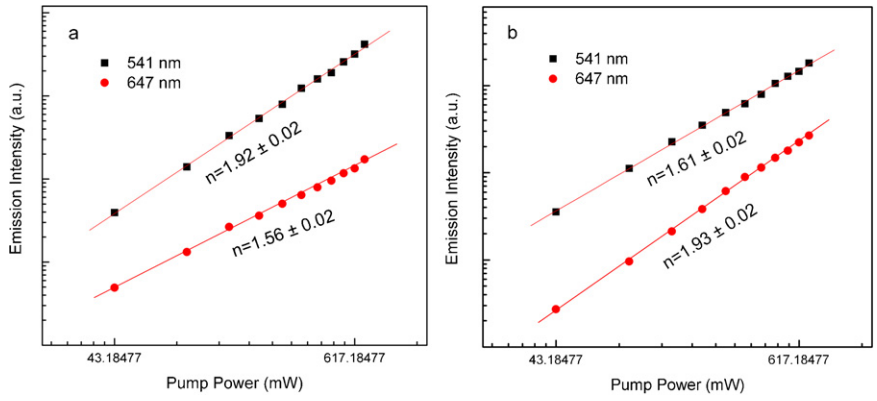

Fig. 5. Pump power dependences of upconversion emissions in (a) $NaYF_4$:Yb^{3+}/Ho^{3+} nanocrystals and (b) $NaYF_4$:Yb^{3+}/Ho^{3+}@SiO_2/Au nanocomposite CN1.

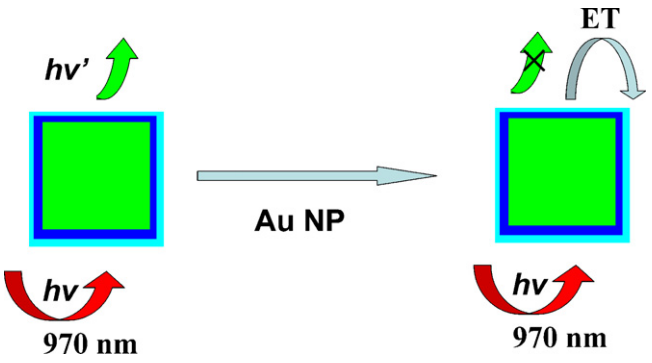

Fig. 6. Schematic illustration for the FRET process between $NaYF_4$:Yb^{3+}/Ho^{3+} upconversion nanocrystals (donor) and gold nanoparticles (acceptor) in the nanocomposite. ET = energy transfer.

CT value than commercial iodinated agent [21]. Through this experiment, we found that $NaYF_4$:Yb^{3+}/Ho^{3+}@SiO_2/Au nanocomposites possess a higher CT value than gold nanoparticles. In addition to their UC luminescence, $NaYF_4$:Yb^{3+}/Ho^{3+}@SiO_2/Au nanocomposites have great potential as multimodality contrast agents.

The colloidal stability and modification of the $NaYF_4$:Yb^{3+}/Ho^{3+}@SiO_2/Au nanocomposites. An important requirement for the widespread use of nanomaterials in biomedicine is that the nanomaterials can maintain stability in the physiological NaCl solution (concentration being 155 mmol/L). Otherwise, the aggregation of nanomaterials could cause unwanted blood vessel blockage. Fig. 8 exhibits the UC emission and photograph of $NaYF_4$:Yb^{3+}/Ho^{3+}@SiO_2/Au nanocomposites CN1 colloidal solution with and without NaCl. The sharp decrease of the UC luminescence intensity suggests that these nanocomposites aggregate when the ionic strength is 90 mmol/L. The nanocomposites aggregated and deposited on the bottom of the bottle. This indicates that the synthesized nanocomposites have a poor colloidal stability in NaCl solution. By checking the colloidal stability of each building block of the nanocomposites, it is found that the building blocks have a totally different colloidal stability. The $NaYF_4$:Yb^{3+}/Ho^{3+}@SiO_2 nanoparticles can be easily dispersed in solution with a high NaCl concentration, while the citrate-stabilized gold nanoparticles easily aggregate in solution with low NaCl concentration due to NaCl sharply decreasing the electric double layer surrounding the gold nanoparticles. Based on the above analysis, we think that the poor colloidal stability of the prepared nanocomposites is induced by the gold nanoparticles weakly protected by citrate. Encapsulating the gold nanoparticles

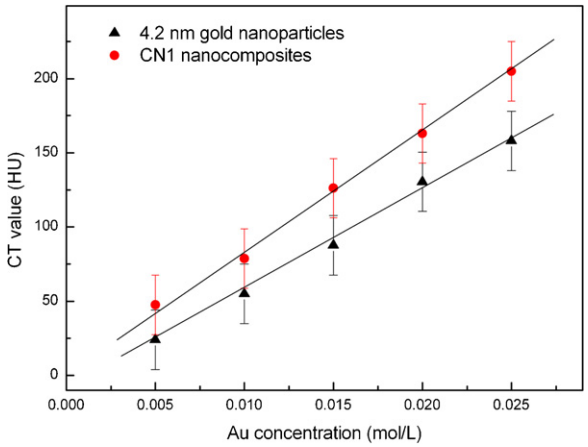

Fig. 7. X-ray attenuation and concentration relation of gold nanoparticles and $NaYF_4$:Yb^{3+}/Ho^{3+}@SiO_2/Au nanocomposite CN1.

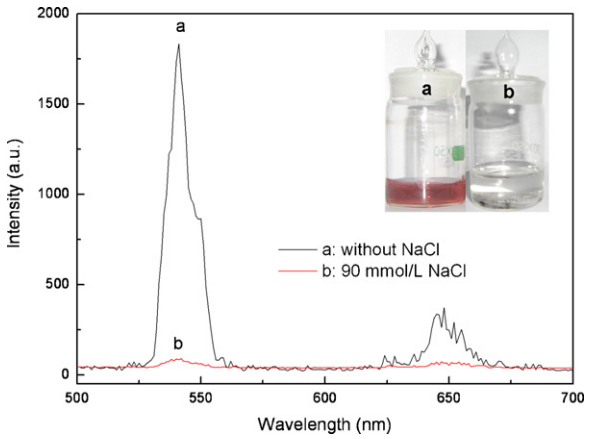

Fig. 8. Upconversion luminescence spectra and photograph (insert) of nanocomposite CN1 diffused in solution (a) without NaCl, and (b) with 90 mmol/L NaCl.

with other stabilizing shell may endow the nanocomposites with a high colloidal stability in NaCl solution.

Gold nanoparticles are easily modified with various molecules, such as thiolate, phosphine, amine, and surfactant. Particularly, thiolate can integrate with gold nanoparticles through a robust Au–S interaction. Thus, we chose 3-mercaptopropionic acid (MPA) as the ligands to replace the citrate absorbed on the gold nanoparticle surface so as to improve the colloidal stability of the nanocomposites. Fig. 9 exhibits the absorption intensity in 531 nm and UC luminescence intensity in 541 nm as well as the photograph of the nanocomposite CN1 modified by MPA molecules when diffused in solutions with different NaCl concentrations. It can be seen that almost no difference can be detected in the absorption intensity and emission intensity as well as the color of the MPA-modified nanocomposites, even with NaCl concentration being as high as 240 mmol/L. Fig. 10 presents the proposed model for the electric double-layer structure of gold nanoparticles stabilized by MPA ligands. The pH value of the NaCl solution is 7.0, which is higher than the pK_a value of MPA (pK_a = 4.87). The deprotonation of –COOH groups would provide a high electrostatic repulsion. Furthermore, the tightly bound thiolate ligands could prevent aggregation by maintaining interparticle repulsion via a steric hindrance. These repulsions lead to the MPA modified gold nanoparticles exhibiting a high colloidal stability, which allows the

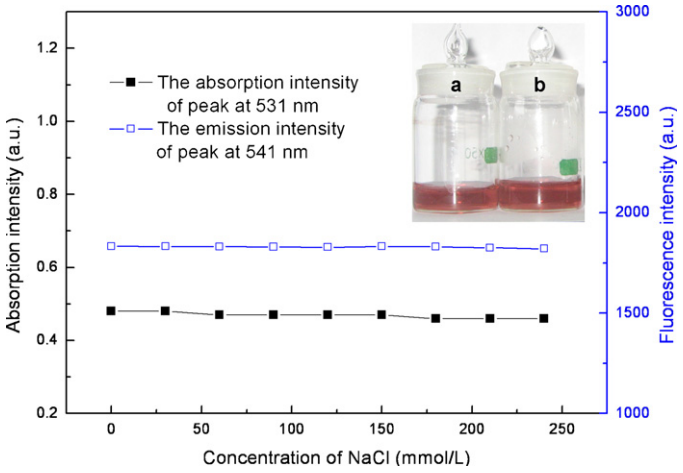

Fig. 9. The absorption intensity in 531 nm and upconversion luminescence intensity in 541 nm as well as photograph (insert) of nanocomposite CN1 modified by MPA molecules when diffused in solutions with different NaCl concentrations. (a) Without NaCl and (b) with 240 mmol/L NaCl.

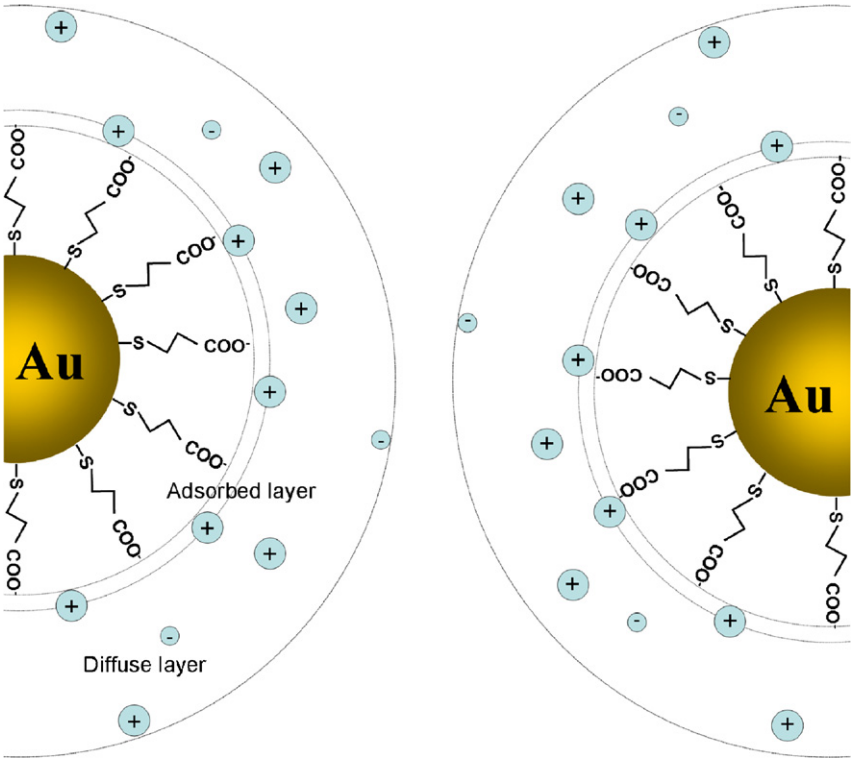

Fig. 10. Schematic illustration of the electric double-layer structure of gold nanoparticles with charged MPA ligands on their surface. The structure consists of gold core, ligand layer, adsorbed layer and diffuse layer.

$NaYF_4$:Yb^{3+}/Ho^{3+}@SiO_2/Au nanocomposites to overcome aggregation and remain stable in a high concentration ionic solution.

4. Conclusions

In summary, bifunctional water-soluble $NaYF_4$:Yb^{3+}/Ho^{3+}@SiO_2/Au nanocomposites are successfully prepared via a facile layer-by-layer technology in which a utility of mercapto–silica shell as a functional layer on central $NaYF_4$:Yb^{3+}/Ho^{3+} nanocrystals and tuning the mole ratio of the Au nanoparticles to the $NaYF_4$:Yb^{3+}/Ho^{3+}@SiO_2 nanoparticles achieve control of the attachment of Au nanoparticles to the nanocomposites. The nanocomposites simultaneously exhibit UC luminescence and high X-ray attenuation. When the gold nanoparticles in the nanocomposites are functionlized with MPA ligands, the nanocomposites exhibit a high colloidal stability even in the presence of 240 mM NaCl. The performance of the prepared nanocomposites and the inherent biocompatibility of the water-soluble gold nanoparticles and silica coated UC nanocrystals create an immense potential for applications as robust multimodality contrast agents for fluorescence imaging and CT scanning. In addition, the attached gold nanoparticles can be easily linked up with targeting molecules and drug molecules, which may have the bifunction of not only increasing the efficiency of molecular imaging but also in situ curing of diseases. Moreover, the facile synthetic strategy of having the ability to engineer gold coverage on particles surfaces allows for controlled biofunctionalization and paves the way for the preparation of diverse bifunctional nanoarchitectures.

Acknowledgment

This work was supported by the Excellent Youth Foundation of Heilongjiang Province of China (no. JC200715).

References

[1] J.M. Nam, C.S. Thaxton, C.A. Mirkin, Science 301 (2003) 1884.
[2] J.G. Zhou, H.T. Fang, J.M. Maley, J.Y.P. Ko, M. Murphy, Y. Chu, R. Sammynaiken, T.K. Sham, J. Phys. Chem. C 113 (2009) 6114.
[3] H.C. Zeng, J. Mater. Chem. 16 (2005) 649.
[4] Q. Sun, X.Q. Chen, Z.K. Liu, F.P. Wang, Z.H. Jiang, C. Wang, J. Alloys Compd. 509 (2011) 5336.
[5] L.S. Zhang, L.Y. Jiang, C.Q. Chen, W. Li, W.G. Song, Y.G. Guo, Chem. Mater. 22 (2010) 414.
[6] F. Wang, Y. Han, C.S. Lim, Y.H. Lu, J. Wang, J. Xu, H.Y. Chen, C. Zhang, M.H. Hong, X.G. Liu, Nature 463 (2010) 1061.
[7] F. Auzel, Chem. Rev. 104 (2004) 139.
[8] G.F. Wang, Q. Peng, Y.D. Li, Chem. Eur. J. 16 (2010) 4923.
[9] F. Wang, X.G. Liu, Chem. Soc. Rev. 38 (2009) 976.
[10] L.Y. Wang, R.X. Yan, Z.Y. Hao, L. Wang, J.H. Zeng, H. Bao, X. Wang, Q. Peng, Y.D. Li, Angew. Chem. Int. Ed. 44 (2005) 6054.
[11] L.Y. Wang, Y.D. Li, Chem. Commun. (2006) 2557.
[12] G.S. Yi, G.M. Chow, Chem. Mater. 19 (2007) 341.
[13] K.Z. Zheng, D. Zhao, D.S. Zhang, N. Liu, F. Shi, W.P. Qin, J. Alloys Compd. 509 (2011) 5848.
[14] Z.Q. Li, L.M. Wang, Z.Y. Wang, X.H. Liu, Y.J. Xiong, J. Phys. Chem. C 115 (2011) 3291.
[15] X.M. Qian, X.H. Peng, D.O. Ansari, Q. Yin-Goen, G.Z. Chen, D.M. Shin, L. Yang, A.N. Young, M.D. Wang, S.M. Nie, Nat. Biotechnol. 26 (2008) 83.
[16] M.E. Stewart, C.R. Anderton, L.B. Thompson, J. Maria, S.K. Gray, J.A. Rogers, R.G. Nuzzo, Chem. Rev. 108 (2008) 494.
[17] N.L. Rosi, C.A. Mirkin, Chem. Rev. 105 (2005) 1547.
[18] M.C. Bowman, T.E. Ballard, C.J. Ackerson, D.L. Feldheim, D.M. Margolis, C. Melander, J. Am. Chem. Soc. 130 (2008) 6896.
[19] Y. Pan, S. Neuss, A. Leifert, M. Fischler, F. Wen, U. Simon, G. Schmid, W. Brandau, W. Jahnen-Dechent, Small 3 (2007) 1941.
[20] N. Lewinski, V. Colvin, R. Drezek, Small 4 (2008) 26.
[21] Z.J. Wang, L.N. Wu, W. Cai, Chem. Eur. J. 16 (2010) 1459.
[22] S. Link, M.A. El-Sayed, J. Phys. Chem. B 103 (1999) 4212.
[23] Z.J. Wang, W. Cai, J.H. Sui, ChemPhysChem 10 (2009) 2012.
[24] N.R. Jana, L. Gearheart, C.J. Murphy, Langmuir 17 (2001) 6782.
[25] G. Mie, Ann. Phys. 25 (1908) 377.
[26] M.C. Daniel, D. Astruc, Chem. Rev. 104 (2004) 293.
[27] G.Y. Chen, H.C. Liu, G. Somesfalean, H.J. Liang, Z.G. Zhang, Nanotechnology 20 (2009) 385704.
[28] J.Q. Gu, L.D. Sun, Z.G. Yan, C.H. Yan, Chem. Asian J. 3 (2008) 1857.
[29] K.E. Sapsford, L. Berti, I.L. Medintz, Angew. Chem. Int. Ed. 45 (2006) 4562.
[30] http://physics.nist.gov/PhysRefData/XrayMassCoef.